

Surface Wave Development and Ambient Sound in the Ocean



Key Points:

- Underwater sound from 1 to 20 kHz is usually associated with wind forcing and the bubbles generated by ocean surface waves
- Considering surface waves in addition to surface winds can improve quantification of underwater sound
- Ambient sound levels are elevated 2–3 dB when waves are developing, relative to fully developed waves at given wind speed

Correspondence to:

J. Thomson,
jthomson@apl.washington.edu

Citation:







Thomson, J., Yang, J., Taylor, R., Rainville, E. J., Zeiden, K., Rainville, L., et al. (2024). Surface wave development and ambient sound in the ocean. *Journal of Geophysical Research: Oceans*, 129, e2024JC021921. <https://doi.org/10.1029/2024JC021921>

Received 30 SEP 2024

Accepted 8 DEC 2024

Author Contributions:

Conceptualization: Jim Thomson
Data curation: Jim Thomson, Jie Yang, Robert Taylor, E. J. Rainville, Luc Rainville, Samuel Brenner, Megan Ballard, Meghan F. Cronin
Formal analysis: Jim Thomson, Megan Ballard
Funding acquisition: Jim Thomson
Investigation: Jim Thomson, Robert Taylor, Megan Ballard
Methodology: Jim Thomson, Robert Taylor, Megan Ballard
Project administration: Jim Thomson
Resources: Jim Thomson
Software: Jim Thomson, E. J. Rainville
Supervision: Jim Thomson
Validation: Jim Thomson, Robert Taylor
Visualization: Jim Thomson, Robert Taylor, Kristin Zeiden
Writing – original draft: Jim Thomson

Jim Thomson¹ , Jie Yang¹, Robert Taylor², E. J. Rainville¹ , Kristin Zeiden¹ , Luc Rainville¹ , Samuel Brenner^{1,3} , Megan Ballard², and Meghan F. Cronin⁴ 

¹Applied Physics Laboratory, University of Washington, Seattle, WA, USA, ²Applied Research Laboratories, University of Texas at Austin, Austin, TX, USA, ³Environmental Science and Engineering, California Institute of Technology, Pasadena, CA, USA, ⁴Pacific Marine Environmental Laboratory, NOAA, Seattle, WA, USA

Abstract Wind, wave, and acoustic observations are used to test a scaling for ambient sound levels in the ocean that is based on wind speed and the degree of surface wave development (at a given wind speed). The focus of this study is acoustic frequencies in the range 1–20 kHz, for which sound is generated by the bubbles injected during surface wave breaking. Traditionally, ambient sound spectra in this frequency range are scaled by wind speed alone. In this study, we investigate a secondary dependence on surface wave development. For any given wind-speed, ambient sound levels are separated into conditions in which waves are 1) actively developing or 2) fully developed. Wave development is quantified using the non-dimensional wave height, a metric commonly used to analyze fetch or duration limitations in wave growth. This simple metric is applicable in both coastal and open ocean environments. Use of the wave development metric to scale sound spectra is first motivated with observations from a brief case study near the island of Jan Mayen (Norwegian Sea), then robustly tested with long time-series observations of winds and waves at Ocean Station Papa (North Pacific Ocean). When waves are actively developing, ambient sound levels are elevated 2–3 dB across the 1–20 kHz frequency range. This result is discussed in the context of sound generation during wave breaking and sound attenuation by persistent bubble layers.

Plain Language Summary Recordings of sound in the open ocean are usually louder when it is windy. This is because winds cause breaking waves at the surface of the ocean (whitecaps), which inject bubbles into the upper ocean. This study introduces wave measurements as a secondary dependence on ambient sound levels. We show that including wave measurements can improve interpretation of sound in the ocean, relative to using wind measurements alone. In particular, sound is loudest when there are a lot of small waves breaking and no larger waves present.

1. Introduction

The relationship between wind speed and the spectral level of ambient sound $S(f)$ in the ocean at mid-frequencies (1–20 kHz) has long been recognized. The classic Wenz (1962) curves have provided decades of prognostic estimates for the so-called ‘wind noise’ that increases with wind speed. Many subsequent updates have followed (Hildebrand et al., 2021), including the recent work of Yang et al. (2023) synthesizing decades of coincident wind and sound observations. Though many sophisticated models now exist for predicting ambient sound levels (Barclay, 2022; Harrison, 1997; Kuperman & Ingenito, 1980; Wilson, 1983), most remain purely parameterized in terms of wind forcing. This traditional approach has the implicit assumption that surface wave breaking and subsequent bubble evolution are uniquely determined by wind speed alone. Yet surface waves develop in response to wind forcing as a function of both time and distance, not as an instantaneous 1:1 relation. Furthermore, the observed reduction in ambient sound under high winds clearly suggests that monotonic wind speed parameterizations are incomplete (D. M. Farmer & Lemon, 1984; Yang et al., 2023). The present study explores surface wave development as a secondary control on ambient sound spectra $S(f)$, removing the implicit assumption of a 1:1 correspondence between surface winds and surface waves.

Although it is still called ‘wind noise’, the literature is clear that the generation mechanism for mid-frequency ambient sound is actually surface wave breaking and subsequent bubble activity (Medwin & Beaky, 1989). This is perhaps best shown at the coasts, where mid-frequency sound production in the surf zone is closely related to incident wave energy (Deane, 2000). In the open ocean, the relation of mid-frequency ambient sound to the dissipation rate of breaking surface waves was shown by Felizardo and Melville (1995). The relationship is

© 2024 The Author(s).

This is an open access article under the terms of the [Creative Commons Attribution-NonCommercial](https://creativecommons.org/licenses/by-nc/4.0/) License, which permits use, distribution and reproduction in any medium, provided the original work is properly cited and is not used for commercial purposes.

Writing – review & editing:
Jim Thomson, Robert Taylor,
Kristin Zeiden, Samuel Brenner

sufficiently clear that prior studies have used ambient sound to detect and quantify breaking waves (D. Farmer & Vagle, 1988; Manasseh et al., 2006).

Surface wave breaking generates bubbles, which both produce and attenuate mid-frequency underwater sound. A wide distribution of bubble sizes is generated within the plume beneath each breaking wave. Bubbles initially pulsate and produce sound at frequencies inversely proportional to their size, then later become acoustically quiescent (Deane & Stokes, 2002). The larger bubbles are buoyant in the turbulent flow and either rise to the surface or collapse. The smaller bubbles do not have sufficient rise velocity and remain submerged (Na et al., 2016). In high sea states, repeated breaking forms a persistent layer of submerged bubbles that can trap sound in a near-surface waveguide (D. M. Farmer & Vagle, 1989) and attenuate sound as it propagates (Ainslie, 2005). This persistent bubble layer has been suggested as the cause of reductions in received levels under high winds (D. M. Farmer & Lemon, 1984; Yang et al., 2023).

The aim of this paper is to further connect ‘wind noise’ to surface wave processes and explore ambient sound as a function of wave development (in addition to wind speed). There are some parallels in this work to the recent results of Dragan-Górska et al. (2023), who show wave dependence on ambient sound levels in the Baltic Sea and discuss differences from classic wind dependence that may be caused by fetch-limitation of the wavefield. In simplest form, the goal of the paper is to provide wave-based adjustments to the classic wind-based Wenz (1962) curves. There remain several dB of scatter in the wind-based curves; we seek a reduction in that scatter by including the degree of surface wave development.

1.1. Surface Wave Development Relative to Wind Forcing

Ocean surface gravity waves do not have simple 1:1 correspondence with local wind speed, though many parametric models assume it (Pierson & Moskowitz, 1964). Rather, surface waves evolve as a balance of energy input from the wind and energy dissipation during wave breaking. There are also nonlinear energy transfers between the different wave frequencies of the wave energy spectrum $E(f)$ (Phillips, 1985). The evolution of the wave spectrum requires both time (i.e., duration) and space (i.e., fetch). For any given observation of $E(f)$, there is a portion of the wave spectrum termed the ‘equilibrium range’ that will have a local balance of wind input and breaking dissipation (Phillips, 1985; Thomson et al., 2013). The rest of the wave spectrum, including the peak of $E(f)$ and any longer swell waves arriving from remote locations, may not be in local balance with the winds. This means that the significant wave height, which is given by the integral over all frequencies as $H_s = 4\sqrt{\int E(f)df}$, is not uniquely determined by wind speed U_{10} . Any 1:1 relationship between H_s and U_{10} is only a regression to mean conditions, and one that obscures the stages of wave development.

The classic metric used to characterize the development of surface gravity waves relative to wind forcing is the non-dimensional wave height,

$$\hat{H} = \frac{gH_s}{U_{10}^2}, \quad (1)$$

which compares the dimensional significant wave height H_s and gravity g to a given wind speed at 10-m reference height U_{10} . When waves are growing and are actively developing relative to a given wind speed, \hat{H} is small. When waves are no longer growing and are ‘fully developed’ relative to a given wind speed, an empirical limit of $\hat{H} \approx 0.15$ is reached (Alves et al., 2003; Pierson & Moskowitz, 1964). Wave breaking occurs during both developing and fully developed conditions, but under fully developed conditions the breaking limits further wave growth. Note that in practice it is possible to exceed the fully developed value of $\hat{H} \approx 0.15$ if swell arriving from distant locations (i.e., non-local forcing) contributes to $E(f)$ at low frequencies.

The non-dimensional \hat{H} is effectively a ratio of the total wave energy spectrum (given by H_s) to the breaking wave activity in the equilibrium range of the wave spectrum (given by U_{10}). When \hat{H} is small, the developing waves are highly forced, and the wind-wave equilibrium range of the wave spectrum contains most of the wave energy. When \hat{H} is large, the fully developed waves have a mature peak, and the wind-wave equilibrium range is only a small portion of the total wave energy spectrum.

Though simple, \hat{H} is a useful metric to separate the wave scales and the processes relevant to the generation and attenuation of ambient sound by bubbles. One of the key observational metrics for wave breaking activity and bubble presence is the whitecap coverage, which has long been tied to wind speed (Brumer et al., 2017; Monahan & Lu, 1990) and more recently tied to the equilibrium range of the wave spectrum (Schwendeman & Thomson, 2015). The wave-breaking literature makes a distinction between stage A whitecaps and stage B whitecaps (Callaghan et al., 2012, 2014; Monahan & Lu, 1990). Stage A whitecaps are actively breaking crests, which are associated with the smaller scales of the surface wave spectrum (i.e., the equilibrium range of the wave spectrum). Stage B whitecaps are the remnant foam that persists after cessation of breaking, which are stretched and transported by the longer scales of the surface wave spectrum (i.e., the peak of the wave spectrum). If sound generation is associated with stage A whitecaps (and small wave scales) and sound attenuation is associated with stage B whitecaps (and large wave scales), then \hat{H} is a proxy for the ratio of sound generation and sound attenuation, as follows.

- The small wave scales and active whitecaps are represented by wind speed in the denominator of Equation 1. These are the wave scales in the equilibrium range of the wave spectrum $E(f)$ (Phillips, 1985), which are directly forced by the winds. These scales are associated with active (stage A) whitecaps (Brumer et al., 2017; Derakhti et al., 2024; Malila et al., 2022; Schwendeman & Thomson, 2015) and the ‘alpha’ bubble plumes described in Monahan and Lu (1990).
- The large scale waves and passive bubble layer are represented by H_s in the numerator of Equation 1, because the total energy in the wave spectrum is concentrated near the peak of the wave spectrum (near wave frequency f_p). The larger peak scales are not directly involved in wave breaking, though they are important to the overall surface kinematics and transport of the subsequent ‘beta’ and ‘gamma’ stages of bubble plumes (Monahan & Lu, 1990).

We acknowledge that peak wave steepness $H_s k_p$ has been used to diagnose wave breaking in the past (M. L. Banner et al., 2000; M. Banner et al., 2002; Thomson et al., 2009), and thus the scales listed above cannot be completely separated. However, recent work has shown that breaking is most active at shorter scales, especially scales at least twice the peak wavenumber k_p of wave energy spectrum $E(f)$ (Kleiss & Melville, 2010; Melville & Matusov, 2002; Schwendeman et al., 2014; Sutherland & Melville, 2013; Thomson et al., 2009).

The analysis that follows tests wave development \hat{H} as a secondary control on ambient sound in the ocean (in the 1–20 kHz range). The analysis begins with a case study to demonstrate this wave scale separation, then expands to a larger data set more suitable to robust statistics. The results focus on wave-based adjustments to wind speed curves for ambient sound spectra, and the attenuation of ambient sound under high winds. We speculate on the bubble dynamics and consider other wave development metrics in the discussion section.

2. Observations

Two data sets, both with measured winds, wave, and ambient sound, are used to explore the relation of mid-frequency ambient sounds to wave development. The first data set is a short-term record, with multiple SWIFT drifters in the Norwegian Sea. The SWIFT drifters were placed at various fetch distances downwind of the Jan Mayen volcanic island; these observations were the original inspiration for the analysis framework described above. The second data set is a long-term record, using 2 years of mooring data from Ocean Station Papa in the North Pacific Ocean. These long-term observations are used for statistical tests of wave development as a secondary determinant of ambient sound. The first data set has the benefit of distributed sampling such that H_s changes without changing U_{10} in Equation 1, while the second data set has the benefit of many realizations. The hydrophone depths are quite different between the two data sets (10 vs. 500 m, respectively). Assuming the ambient sound source behaves as a dipole, the acoustic spreading loss resulting from a greater receiver depth is offset by the increased number of contributing surface sources (Urick, 1975). Therefore, after taking out water absorption, the two data sets are comparable.

2.1. Jan Mayen Drifters

Jan Mayen is a volcanic island at the west edge of the Norwegian Sea, surrounded by a narrow shelf and deeper ridge separating the Greenland Basin from the Lofoten Basin. Data from this location were collected as part of a 2021 pilot cruise for the Northern Ocean Rapid Surface Evolution (NORSE) project (M. Ballard et al., 2022).

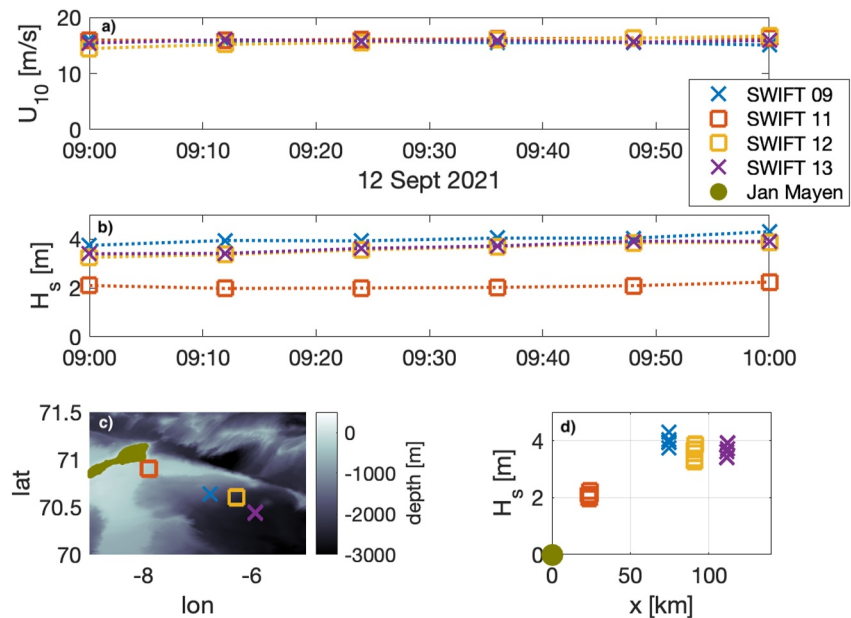


Figure 1. Time series of (a) wind speeds, (b) significant wave heights, and (c) positions (lower left panel) of drifting SWIFT buoys near the island of Jan Mayen. Shading in the lower left panel indicates water depth (green is land). The wind speeds are similar for all buoys, while the wave heights are a strong function of the fetch distance X downwind of the island (d).

Data were collected with drifting SWIFT buoys (Thomson, 2012), which measure winds, waves, and turbulence in a wave-following reference frame. For these deployments, two of the SWIFTs included a Loggerhead SNAP hydrophone suspended at a depth of 10 m. The SNAP hydrophone spectra used herein come from recordings that are 60 s in duration, at an interval of 300 s. The acoustic sampling rate is 48 kHz. The SNAP hydrophone is mounted in a downward orientation, causing the coupled interaction between the electronics housing and the hydrophone, resulting in anomalous features in the acoustic spectra that were especially evident in the 0.9–2.0 kHz band. This is discussed at length in Appendix, and these bands are interpolated across in the results that follow.

The NORSE 2021 pilot experiment sampled a particularly strong wind event on 12 September 2021, during which four SWIFT buoys were deployed at increasing fetch distances downwind of Jan Mayen. The island acted as a barrier to surface waves, such that the fetch is effectively zero at Jan Mayen and increases with distance from the island. As a practical application of this fetch dependence, the R/V Neil Armstrong took shelter within the short fetch behind Jan Mayen during the most intense portion of the wind event. Figure 1 shows the wave and wind conditions measured by the four buoys. For the one-hour time series used in this case study, the wind is nearly constant at $U_{10} = 15$ m/s for all of the buoys, but the wavefield is a strong function of fetch distance X . This creates a natural laboratory for studying wave development.

2.2. Ocean Station Papa (North Pacific) Moorings

Ocean Station Papa is located at 50°N, 145°W in the North Pacific Ocean and has produced one of the longest time series in the world's oceans. Data from this location extend back to the World War II era (Freeland, 2007), including a remarkable data set of visual wave observations (Belka et al., 2014). The modern data at Station Papa are centered around a series of moorings, including a Datawell waverider maintained by the Applied Physics Laboratory at the University of Washington (Thomson et al., 2013, 2015) and a surface meteorological/upper ocean mooring maintained by the Pacific Marine Environmental Laboratory at the National Oceanographic and Atmospheric Administration (NOAA) (Cronin et al., 2015, 2023). The waverider mooring has been replaced every 1–2 years and usually has included a Passive Aquatic Listener (PAL) at 500 m depth. For this study, we select the period of 2010–2012 and utilize the ambient sound recordings and wave data from the waverider mooring, along with the winds from the NOAA mooring.

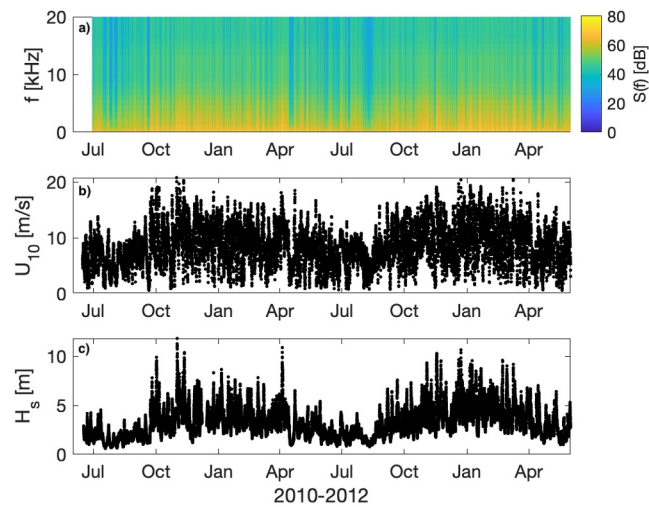


Figure 2. Time series of observations at Ocean Weather Station Papa (Station Papa) from 2010 to 2012. (a) Acoustic spectra are measured with a sub-surface PAL. (b) Wind speeds are measured with anemometers on the NOAA surface buoy. (c) Significant wave heights are measured with a Datawell waverider buoy.

Figure 2 shows the 2010–2012 time series from Station Papa, which has a strong seasonal signal of winter storms and mild summer conditions. All parameters are statistical measures produced hourly: the ensemble ambient sound spectra, the significant wave height from the integral of the wave energy spectra, and the average wind adjusted to 10 m reference height. The ensemble sound spectra come from recordings that are 4.5 s in duration at an interval of 8 min. The acoustic sampling rate is 100 kHz. The recordings are split into 450 windows with 50% overlap, and then spectra from these windows are averaged to produce ensemble spectra every 8 min.

3. Results

3.1. Fetch-Limited Case Study at Jan Mayen

One common application of non-dimensional wave height \hat{H} is the analysis of wave growth along a fetch distance X , which is similarly non-dimensionalized as $\hat{X} = \frac{gX}{U_{10}^2}$. Numerous studies have shown a power-law relation between \hat{H} and \hat{X} (Dobson et al., 1989; Fontaine, 2012; Schwendeman et al., 2014; Stiassnie, 2012; Thomson & Rogers, 2014). Figure 3 shows the wave conditions scaled by the non-dimensional fetch distance downwind of

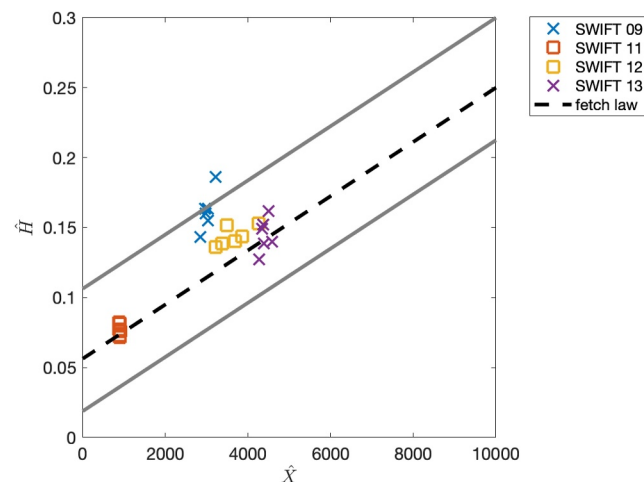


Figure 3. Non-dimensional wave height versus non-dimensional fetch during the Jan Mayen case-study. The dashed line shows the theoretical growth of waves with fetch, assuming steady-state winds and the absence of swell. Gray lines show the range of literature values around the theoretical fetch relation.

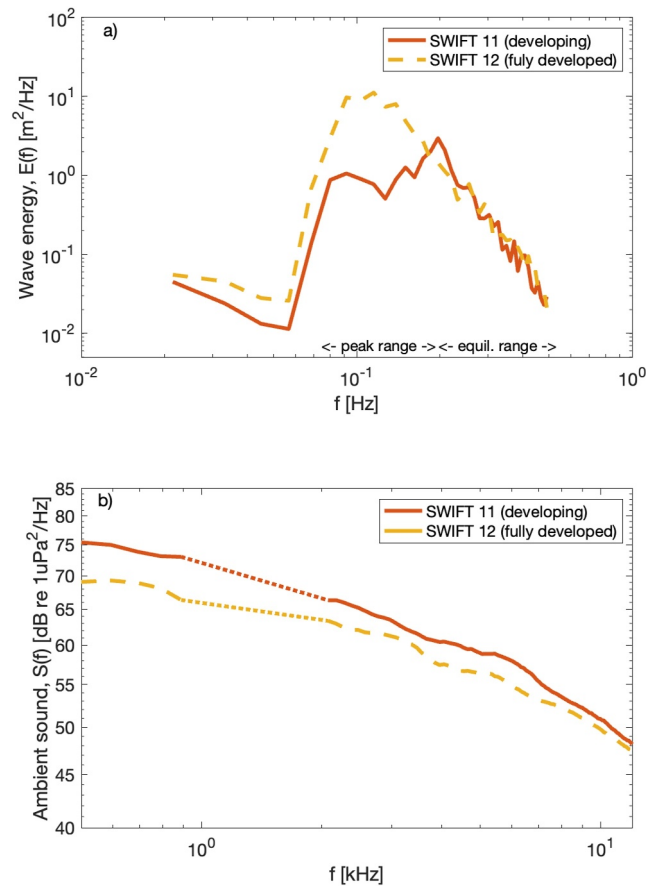


Figure 4. Spectra from the two SWIFT buoys during the Jan Mayen case study. (a) Surface wave spectra, which have similar levels in the equilibrium range but very different peaks. (b) Acoustic spectra, which differ several dB despite observing the same wind speed at both buoys. The dotted portion of the acoustic spectra are frequencies affected by directionality of the receiver (see appendix).

Jan Mayen. The expectation is a quasi-linear, or a weak power-law, relation between the non-dimensional variables (Fontaine, 2012; Stiassnie, 2012), which is shown by the dashed line and bounded by the gray lines in Figure 3. The bounds of the expected fetch relation come from the range of reported values in the literature for the exponent b in $\hat{H} = a\hat{X}^b$.

Figure 3 makes it clear that the differences in wave heights between SWIFT 11 and SWIFT 12 (which have the two hydrophones) are reasonable given the differences in fetch. The observations from this case study are more complex than the classic fetch law, and this is probably because the island does not completely block all of the waves generated upwind of the island. The point is not to achieve a perfect fetch scaling, but rather to explain how these concurrent measurements can have very different stages of wave development.

The scalar wave energy spectra $E(f)$ shown in Figure 4a provide a more complete description of wave development along the fetch. Both wave spectra have similar levels in the high-frequency tail (i.e., the equilibrium range where most of the wave breaking occurs). At lower frequencies, the wave spectra differ dramatically. At short fetch (SWIFT 11), the peak is narrow and most of the wave energy is within the equilibrium range, as noted by the f^{-4} shape (Thomson et al., 2013). At long fetch (SWIFT 12), the peak contains most of the energy, though the wind-wave equilibrium range is still present (as expected, given that the buoys measured the same wind speed). These wave spectra also suggest that there is minimal propagation of longer waves around the island, because the wave spectra do not have a discernible second peak at low frequencies (as would be expected for swell).

The contrasting wave spectra demonstrate the general usage of \hat{H} as a ratio of the energy associated with breaking waves to the energy at longer wave scales. SWIFT 11 has $\hat{H} = 0.06$, which is well within the developing range.

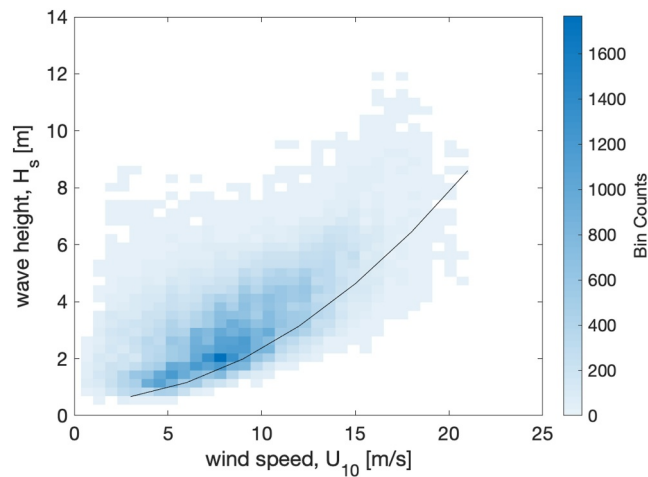


Figure 5. Histograms of significant wave height at Station Papa versus wind speed. The bin counts are observations at hourly intervals over 2 years. The black curve shows the (dimensional) fully developed threshold ($\hat{H} = 0.15$). Observations with wave heights below this line are developing waves.

SWIFT 12 has $\hat{H} = 0.15$, which is the expected value for fully developed waves. In developing waves, the wind-wave equilibrium range contributes much of the total energy and U_{10} sets the level. In fully developed waves, the peak contributes most of the total energy that determines H_s , even though the equilibrium range is still present.

Figure 4b shows ambient sound spectra $S(f)$ from the same two SWIFTs downwind of Jan Mayen. The two spectra are notably different. At short fetch (SWIFT 11, $\hat{H} = 0.06$), measured sound is elevated several dB relative to the measurements at long fetch (SWIFT 12, $\hat{H} = 0.15$). This dB difference is quasi-uniform across the frequency range 1–20 KHz, though it narrows somewhat above 10 kHz. This narrowing of the dB difference is notable because the data are from winds speeds ($U_{10} \approx 18$) at which high-wind sound attenuation is thought to emerge (D. M. Farmer & Lemon, 1984; Yang et al., 2023).

Given the uniform wind forcing and similar wind-wave equilibrium range in the wave spectra, we can hypothesize that sound generation is the same for both buoys. The difference in received ambient sound might thus be additional sound attenuation by a thicker layer of persistent bubbles with the larger H_s (i.e., at greater fetch where the waves are fully developed). An alternate hypothesis regarding the difference in water depth between these locations is addressed in the Discussion section; modeling suggests that water depth is insufficient to cause a 3–5 dB change between these buoys. Further, the ambient sound dependence on fetch (and thus wave development) shown here is qualitatively similar to the recent results of Dragan-Górska et al. (2023) in the Baltic Sea.

3.2. Station Papa Results

The 2-year data set from Station Papa provides ample observations to populate wind speed bins of traditional Wenz (1962) curves and then further separate each bin into wave development categories. Though there is no fetch limitation at this site, there are still cases where waves are not fully developed (because of finite wind duration). There are also cases in which the waves exceed the fully developed threshold, which are cases with strong swells generated by winds at other locations. Figure 5 shows a binned joint histogram of dimensional wave heights and wind speeds. The conditions are often fully developed and greater, but there are several hundred observations of developing waves spanning all wind speeds. Overall, the developing cases are about 5% of the total record.

Figure 5 shows clearly that assuming a 1:1 relation of wind speed and wave height is incomplete. The figure also shows that the choice of $\hat{H} = 0.15$ as the fully developed criteria may be imperfect, though it is not meant to divide the joint histogram in half. Rather, \hat{H} is meant to quantify when the wave energy is mostly in the wind-wave equilibrium range or when the wave spectrum is mostly in the peak range.

Figure 6 shows ensemble ambient sound spectra $S(f)$ from Station Papa binned by wind speed (as in the Wenz curves), with additional sub-bins for developing and fully developed waves. The sorting by wind speed bins is

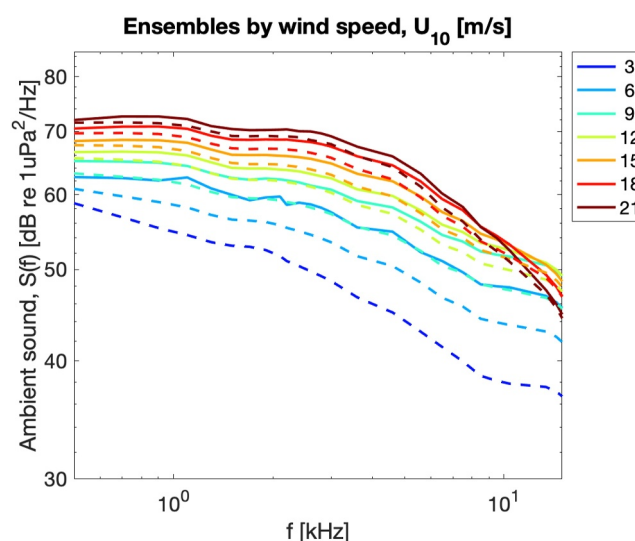


Figure 6. Ensemble acoustic spectra from 2 years of data at Station Papa that are binned by wind speed. The solid curves are developing waves ($\hat{H} < 0.15$) and the dashed curves are fully developed ($\hat{H} \geq 0.15$).

qualitatively similar to Yang et al. (2023), including the reduction in sound at high frequencies during high winds. The separation into wave categories provides a further sorting, in which developing wave conditions are consistently louder than fully developed conditions. This is consistent with the fetch-limited case study at Jan Mayen.

In many cases, the separation by wave conditions at a given wind speed leads to a change in magnitude that is similar to the difference between neighboring wind speed bins (i.e., a few dB). Thus the wave-based adjustment to classic wind noise curves might seem modest, but it is appreciable relative to the scatter in existing wind speed curves (Yang et al., 2023). The standard error of the ensemble mean in each bin is less than 0.1 dB for all bins. These error bars are not shown in Figure 6 for visual simplicity; they are sufficiently small that the observed differences between each line are statistically significant at 95% confidence (and often at 99% confidence).

Figure 7 shows the wind (and wave) dependence of ambient sound at select acoustic frequencies. This is a visually simpler presentation of the same binned ensembles in Figure 6. At 1.5 kHz, there is a monotonic increase in sound level with wind speed, and sound is approximately 1 dB louder for developing waves relative to fully developed. At 7.5 kHz, sound levels increase at moderate winds, but appear to saturate at higher winds. The difference related to wave development is 2–3 dB. At 15 kHz, the difference related to wave development is 2–3 dB at moderate winds, but narrows to less than 1 dB at high winds where sound levels have a notable decrease. The decrease in received sound at high winds is similar to the recent results of Yang et al. (2023), but here the scatter is reduced by including the degree of wave development. The convergence of the wave development curves at high winds and high acoustic frequencies hints at the bubble dynamics related to sound attenuation. It may be related to the wave dynamics, following the recent study of (Davis et al., 2023) showing the compression of the equilibrium range for winds above 18 m/s.

4. Discussion

Here we interpret the empirical result that sound levels are consistently reduced when surface waves are fully developed at a given wind speed. Measured ambient sound in the ocean is the net effect of sound production and sound attenuation, and thus discussion must consider both processes. We speculate below that wave development \hat{H} is a proxy ratio comparing scales of sound attenuation and scales of sound production. Both portions of this ratio are related to bubble plumes in the upper ocean. This study did not include direct measurements of bubble plumes, so we can only build an interpretation based on the available literature. We build our interpretation on the work of Czerski et al. (2022), who describe the ocean in terms of two distinct bubble layers: a shallow layer directly related to wave breaking and a deeper layer related to circulation patterns.

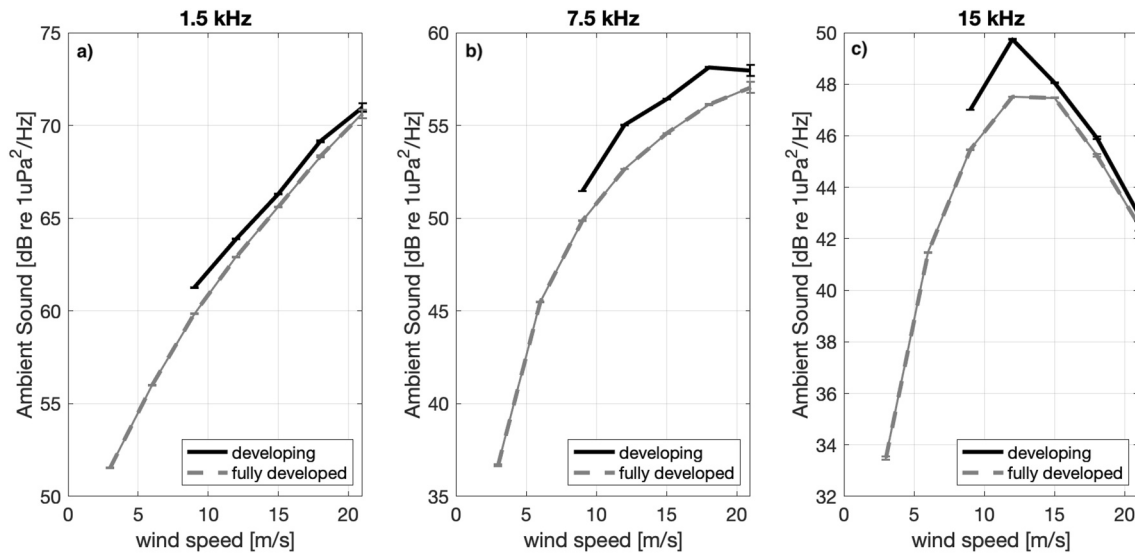


Figure 7. Ambient sound level versus wind speed for select acoustic frequencies (a) 1.5 kHz, (b) 7.5 kHz, and (c) 15 kHz. The solid curves are developing waves ($\hat{H} < 0.15$) and the dashed curves are fully developed ($\hat{H} \geq 0.15$). Vertical bars show the standard error in each bin, but they are always less than 0.1 dB and thus not visible.

4.1. Whitecaps, Wind Speed, and Sound Production

The empirical result that ambient sound is *louder* for developing wave conditions, rather than fully developed waves, might seem counter-intuitive. Yet we should expect that the smaller waves produce more sound than the larger waves, because it is the smaller waves that are directly forced by the winds and do most of the breaking. The literature is clear that wave breaking activity primarily occurs at wavenumbers much higher (i.e., scales much smaller) than the peak of the wave energy spectrum (Kleiss & Melville, 2010; Melville & Matusov, 2002; Schwendeman et al., 2014; Sutherland & Melville, 2013; Thomson & Jessup, 2009). This is corroborated by the results of Schwendeman and Thomson (2015) and also Derakhti et al. (2024), who show that whitecap coverage is strongly dependent on the steepness of the short waves (in equilibrium with the wind forcing) but mostly independent on the long waves. The whitecaps, in turn, are directly related to the near-surface bubbles that generate sound (Monahan, 1993).

The common assumption of a 1:1 relation between winds and waves is only applicable within the equilibrium range of the wave spectrum. Indeed, the equilibrium range of the wave spectrum is now routinely used to estimate wind speed from wave observations when direct measurements are not available (Voermans et al., 2019). This suggests that the traditional use of U_{10} as a proxy for sound production associated with whitecaps is a valid approach, but that other wave scales may be important to sound attenuation.

Revisiting the wave energy spectra in the fetch-limited case study (Figure 4a), breaking activity predominately occurs in the equilibrium range of wave scales, which is similar between the two spectra. This suggests that wave breaking and sound production might be the same between the two cases, especially given the similar wind speed. If this were true, the difference in observed sound levels would need to arise from differences in sound attenuation.

4.2. Wave Height, Bubble Layers, and Sound Attenuation

As described in detail by D. M. Farmer and Lemon (1984) and reinforced by Yang et al. (2023), the layer of persistent bubbles below the ocean surface can absorb sound and cause attenuation of measured ambient sound levels at depth. The emergence of strong attenuation at high winds (Figure 7) is likely related to increases in the depth of this bubble layer. Here we make a further link to wave development.

Recent observations from several independent studies indicate that bubble plume penetration depths are well correlated with dimensional H_s , extend to 2–3 factors of H_s beneath the surface, and have temporal persistence of many wave periods (Benetazzo et al., 2024; Cifuentes-Lorenzen et al., 2023; Czerski et al., 2022; Derakhti

et al., 2024; Peláez-Zapata et al., 2024; Strand et al., 2020). The very recent work of Peláez-Zapata et al. (2024) notes a “transition toward stronger and more organized bubble entrainment events during higher wind speeds.” It is common for bubbles to reach at least 10 m depths during high winds (Derakhti et al., 2024) and the smaller bubbles can persist for hours (Czerski et al., 2022). The kinematics of these bubble plumes is thus likely dependent on the *total* wave spectrum, even though the breaking is mostly dependent on the high-frequency portion of the wave spectrum. It is plausible that a more developed wavefield (with larger H_s) drives more vertical transport of the smaller, persistent bubbles. In particular, more developed wave fields will have strong Langmuir forcing that may enhance vertical transport (D’Asaro et al., 2014; Peláez-Zapata et al., 2024), because the Stokes drift scales with wave height and peak frequency (in the monochromatic version) or the third moment of the wave energy spectrum (in the broadband version).

4.3. Other Wave Development Metrics

The \hat{H} metric can be related to other indicators of wave development, such as non-dimensional wave age. Wave age is the ratio of phase speed at the peak of the energy spectrum to wind speed c_p/U_{10} , and has been correlated with the depths of persistent bubble plumes (Peláez-Zapata et al., 2024). Wave age is related to \hat{H} , because both dimensional significant wave height H_s and peak wave period T_p increase as waves develop. At a given wind speed, the increase in T_p will also increase the phase speed c_p , according to linear dispersion. The linkage is more clear considering the non-dimensional wave period $\hat{T} = \frac{gT_p}{U}$ which also increases as wave develop. The distinction is that \hat{H} separates the small and larger waves scales, while wave age is a parameter that is solely defined by the peak. Thus, \hat{H} provides a some of the information that would come from more nuanced spectral partitioning (Portilla-Yandún et al., 2016), while retaining the simplicity of using standard bulk parameters.

Our emphasis on \hat{H} and the importance of the wind-wave equilibrium range (as opposed to peak scales) may provide some hints for future work under high wind conditions. Recent work has shown that the equilibrium range becomes an increasingly narrow portion of the wave spectrum at winds above 18 m/s (Davis et al., 2023). At these high winds, a saturation range emerges in the tail of the wave spectrum, and this indicates wave breaking is the dominant process in the wind-wave balance. These are the conditions in which breaking and bubble production are nearly continuous (as opposed to episodic), such that there will be a nearly constant supply of the persistent bubbles that attenuated sound.

4.4. Shallow-Water Effects Near Jan Mayen

In contrast to the deep-water conditions of Station Papa, the bathymetry around Jan Mayen is complex and includes shallow regions close to the island (Figure 1). The location of SWIFT 11 relative to Jan Mayen and the direction of the wind results in both a shorter fetch and a shallower water depth than that of SWIFT 12. Shallow water depths are frequently associated with elevated ambient acoustic spectra (Wenz, 1962). Wenz considered depths less than 100 fathoms (~ 200 m) to be shallow water. Note that this is ‘shallow water’ in terms of the acoustics, but not in terms of the surface gravity waves. At 200 m, much of the surface gravity wave spectrum is in deep water, though the longer swells are intermediate water depth. At a water depth of ~ 250 m over the duration of the measurements presented, SWIFT 11 is near the transition depth for acoustics defined by Wenz. Wenz suggested adding 2–3 dB to the average empirical wind noise curves in such environments. This suggestion may actually have been masking a wave development dependence, since waves are often less than fully developed in shallow coastal regions. We use an acoustic model to test for shallow water effects, relative to wave development effects.

A range-independent ambient acoustic model was implemented to investigate the influence of the water depth on the ambient sound level (see Appendix for details). The ray-based model traces the propagation paths that arrive at the receiver for a range of elevation angles $-90^\circ < \theta < 90^\circ$. The model provides the incoherent contribution of all surface dipole sources that reach the receiver, accounting for acoustic absorption and reflection losses along each path. The model does not include surface losses or attenuation of sound by persistent bubble layers. Other than water depth, the model environmental inputs for SWIFT 11 and SWIFT 12 were kept the same. The model results suggest at most a difference of 1 dB between the two buoys, which is insufficient to explain the observed differences.

The historical measurements of Lemon et al. (1984) are also relevant to the question of shallow water effects and the possible importance of wave development. That study found elevated ambient sound levels at a coastal site, relative to open ocean levels, for a range of wind speeds (APL-UW, 1994). Although that study did not include wave measurements or consider wave effects, we can review the wind record and estimate that the storm duration was too short to produce fully developed waves. We can also examine the site and assert that refraction along the coast may have further reduced the wave heights. Applying the scaling of our present study, \hat{H} would be smaller for Lemon et al. (1984) than fully developed conditions. Thus, it would make sense for ambient sound levels to be elevated in that study, though we cannot definitively show wave development as the cause.

5. Conclusions

Mid-frequency ambient sound in the ocean is due to surface wave breaking and the generation of bubble plumes in the upper ocean. Consistent with the literature, this work confirms a primary dependence on wind speed (as a parametric representation of this process). This work investigates a previously unexplored secondary dependence on the degree of surface wave development. When waves are still actively developing under a given wind forcing, the ambient sound levels are elevated a few dB relative to when waves are fully developed. We postulate that this relationship is due to the combined effects of sound production by active wave breaking and sound attenuation within the layer of persistent bubbles that forms below the surface, though more observations are needed to verify this mechanism. Relating the state of wave development to the bubble dynamics is a promising approach to explore scale dependence in the reduction of sound levels at high winds (>15 m/s). For the common inverse problem of obtaining proxy winds (and rain rates) from ambient acoustic measurements (Vagle et al., 1990), the results herein provide a framework to explore the scatter in those methods and potential avenues to improve those estimates by a few dB.

Appendix A: Directionality of Loggerhead SNAP Recorders

The time-averaged ambient sound spectra collected with the Loggerhead Snap recorders showed evidence of anomalous features. The most severe features were in the 900 Hz to 2 kHz band, which were removed from Figure 4b and replaced with a dashed line representing an interpolation over the affected frequency band. These features were present throughout the data set, independent of wind speed and wave height. These irregularities in the ambient sound spectra were attributed to the acoustic response of the Snap recorders due to the proximity of the hydrophone to the air-filled pressure housing.

The Snap recorder has a PVC housing roughly 0.5 m long and 5 cm in diameter, with the power supply and data acquisition system contained internally. The external HTI 96 hydrophone is connected to the housing by a 3 cm long semi-rigid cable. The proximity of the hydrophone to the housing, the deployed orientation with the hydrophone pointed away from the sea surface, shadowing and diffraction around the housing, and the acoustic resonances of the cavity are all possible contributing factors to the irregularities observed in the measurements.

To determine the acoustic sensitivity of the Snap recorder as a function of direction and frequency, calibrated measurements were taken at the Lake Travis Test Station in Austin, Texas. The lake bed below the test station has a gradual slope, with an average water depth of 20 m directly below the experimental setup. During testing, the water column consisted of a 30 °C isothermal layer in the upper 12 m, followed by a thermocline reducing the temperature to 20 °C at 20 m. The response of the system is assumed to be symmetric about the axis of the recorder. To measure the change in response as a function of receive angle θ of the incident sound wave, the Snap recorder was suspended horizontally by 10 m of fishing line, with its axis parallel to the water surface. The fishing line was connected to a rotating column, with the hydrophone centered on the column's axis of rotation.

The Snap recorder collected data continuously at 48 kHz as it was rotated at a speed of approximately 1 deg/s, with the 360° rotation lasting roughly 6 min. A Navy standard J9 projector (https://www.navsea.navy.mil/Portals/103/Documents/NUWC_Newport/USRD/J9.pdf) was used for the calibration. It was placed at 10 m depth 1 m from the center of the rotating column. For the J9 projector, far-field propagation is attained roughly 10 cm from the source. The calibration signal was a 10 ms linear frequency modulated chirp from 50 Hz to 20 kHz, repeated every 250 ms. The length of the chirp was chosen to prevent reflections from contaminating the received signal.

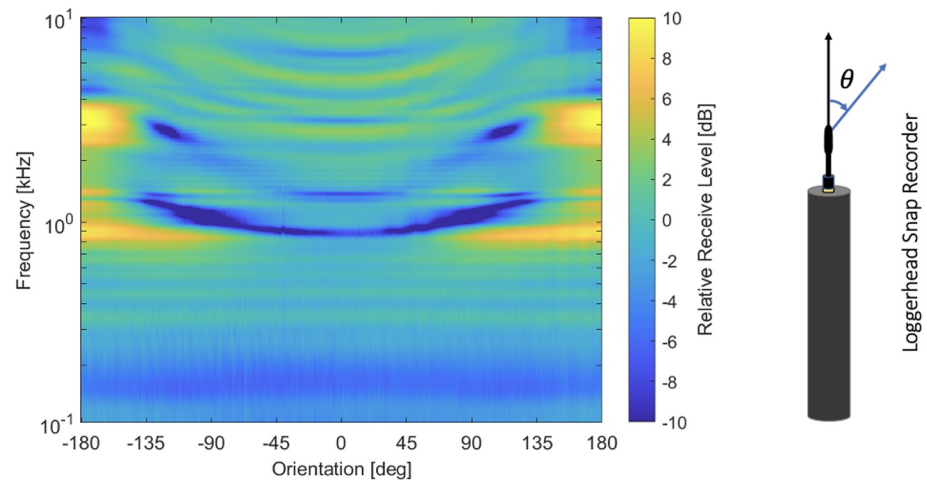


Figure A1. Measured acoustic directivity of the Loggerhead Snap recorder. Positive/negative dB levels indicate the amplification/suppression of received signals at each receiver orientation angle (hydrophone facing source at $\theta = 0^\circ$).

Reference measurements of the projector signal were collected with a calibrated Navy standard H56 hydrophone (https://www.navsea.navy.mil/Portals/103/Documents/NUWC_Newport/USRD/H56.pdf) placed at 10 m depth below the rotating column, that is, in the location previously occupied by the Snap recorder hydrophone. The difference of the received power spectral density level as measured by the reference hydrophone to that measured by the Snap recorder provides the nominal response of the Snap recorder for each receive angle. Figure A1 shows the calibrated acoustic response of the Snap recorder as a function of angle and frequency for the full rotation. Note that a 200 Hz high-pass filter was applied to both the Snap recorder data and the H56 data to remove environmental noise.

The directivity of the Snap recorder is significant, with variations of ± 10 dB at different orientations for many frequencies in the 500 Hz to 4 kHz band. With the deployed orientation facing away from the sea surface, direct path sea surface sound arrives at angles $|\theta| \geq 90^\circ$, with sound from directly overhead arriving at $|\theta| = 180^\circ$ and surface generated sound from more distant patches arriving at lower angles. The strong frequency-dependent directionality is an important consideration in the interpretation of ambient sound data collected with the Snap recorders. Compared to the HIFEVA model ambient sound curves (APL-UW, 1994), the spectra shown in Figure 1b are biased toward higher ambient sound levels. This result is broadly consistent with the measured directivity shown in Figure A1, which on average shows a higher response in the 500 Hz to 4 kHz range for angles between $\pm 90^\circ$ and $\pm 180^\circ$.

Although only one Snap recorder was calibrated at the Test Station, the overall angle- and frequency-dependence is expected to be consistent between units owing to their similar construction. However, the two Snap recorders used for the NORSE ambient sound measurements showed high-frequency oscillations that were slightly offset from one another between 900 Hz and 2 kHz. These oscillations roughly align with the narrow-band, wide-angle elevated response near 1 kHz in the calibration measurement shown in Figure A1. Slight variations in the construction and preparation of the Snap recorders could be responsible for small shifts in the characteristics of the acoustic response. These features were removed from Figure 4b to facilitate a cleaner comparison between the two recorders. While the absolute values of the measurements are influenced by the acoustic response of the recorders, the differences in the observed ambient sound levels between SWIFT 11 and SWIFT 12 can be attributed to differences in the ambient sound generation and propagation environment.

Appendix B: Shallow Water Modeling Near Jan Mayen

The empirical Wenz level N_w , a function of both wind speed U and frequency f , was used for the surface dipole strength $N_w \sin \theta/\pi$. The normalization of the surface dipole strength by π enables a return to the input ambient level N_w when integrating over solid angle in a lossless and bottomless isotropic-sound-speed environment (Ainslie, 2010; APL-UW, 1994), representing the acoustic level as measured by an omnidirectional hydrophone.

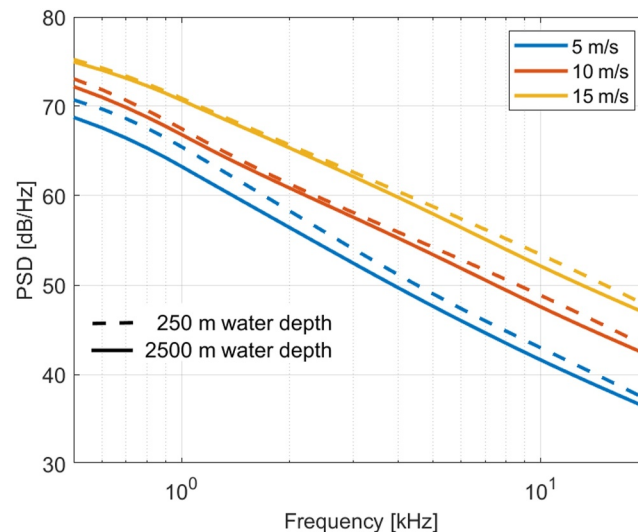


Figure B1. Modeled ambient acoustic spectra for shallow-water and deep-water environments for multiple wind speeds. Increases to the ambient level resulting from the shallower environment are on the order of ~ 1 dB and decrease with increasing wind speeds.

Following the work of M. S. Ballard et al. (2023), the bottom was modeled as a gravel sediment halfspace, providing a fairly reflective fluid bottom with a critical grazing angle of $\sim 30^\circ$. Reflection losses from sea surface interactions were calculated using Ainslie's mid-frequency model (Ainslie, 2005). The sound speed profile used contained a surface duct in the upper 50 m of the water column consistent with measured sound speed profiles from the experiment. Model results for the two different environments for several wind speeds are displayed in Figure B1.

In the shallow water environment, the low-loss gravel bottom intensifies the contribution of small grazing angle energy near horizontal that propagates over long distances. However, the modeled differences in spectral level shown in Figure B1 are not significant enough to explain the measured differences between SWIFT 11 and SWIFT 12, particularly at high wind speeds, where the increase in surface loss prohibits long distance propagation, negating the impact of the reflective bottom. The model's inability to represent the increased ambient acoustic spectral levels measured at SWIFT 11 for the associated wind speeds indicates that water depth is not responsible for the raised levels.

This modeling analysis supports the interpretation that differences in the ambient sound levels are the result of differences in the surface wave development at the two locations. The significant wave heights at SWIFT 11 are much less than those of fully developed conditions in the open ocean (Hasselmann et al., 1973; Pierson & Moskowitz, 1964), because there is insufficient fetch to develop the lower frequency surface waves.

Data Availability Statement

The complete data and processing codes from this work are publicly available at <http://hdl.handle.net/1773/51039>, which is cited as Thomson (2024). Additional processing codes for the SWIFT wave and wind data are in Thomson et al. (2024). Station Papa wind data were retrieved from <https://www.pmel.noaa.gov/ocs/Papa>. Station Papa wave data were retrieved from <http://thredds.cdip.ucsd.edu/thredds/catalog/cdip/archive/166p1/catalog.html> and cited as CDIP (2024).

References

- Ainslie, M. A. (2005). Effect of wind-generated bubbles on fixed range acoustic attenuation in shallow water at 1–4 kHz. *Journal of the Acoustical Society of America*, 118(6), 3513–3523. <https://doi.org/10.1121/1.2114527>
- Ainslie, M. A. (2010). *Principles of sonar performance modelling* (Vol. 707). Springer.
- Alves, J. H. G. M., Banner, M. L., & Young, I. R. (2003). Revisiting the Pierson–Moskowitz asymptotic limits for fully developed wind waves. *Journal of Physical Oceanography*, 33(7), 1301–1323. [https://doi.org/10.1175/1520-0485\(2003\)033<1301:RTPALF>2.0.CO;2](https://doi.org/10.1175/1520-0485(2003)033<1301:RTPALF>2.0.CO;2)
- APL-UW. (1994). High-frequency ocean environmental acoustic models handbook (Tech. Rep. No. TR9407). *Applied Physics laboratory*.

Acknowledgments

This research was supported by the Office of Naval Research (Awards N00014-20-1-2417 and N00014-21-1-2743). The waverider mooring at Ocean Station Papa is maintained using NSF support (award OCE-2122317) and the surface wind mooring at Ocean Station Papa is maintained by NOAA PMEL through funding from NOAA's Global Ocean Monitoring and Observing program. This is PMEL paper number 5604.

- Ballard, M., MacKinnon, J., Rainville, L., Simmons, H., Abbot, P., Bergentz, K., et al. (2022). Northern ocean rapid surface evolution (norse): Science and experiment plan (Tech. Rep. No. 2102). *Applied Physics Laboratory*. University of Washington.
- Ballard, M. S., Sagers, J. D., Poulain, P.-M., Mackinnon, J., Lucas, A. J., & Sanchez-Rios, A. (2023). Out-of-plane arrivals recorded by drifting hydrophones during the northern ocean rapid surface evolution experiment. *Journal of the Acoustical Society of America*, 154(5), 2757–2768. <https://doi.org/10.1121/10.0022052>
- Banner, M., Gemmrich, J., & Farmer, D. (2002). Multiscale measurements of ocean wave breaking probability. *Journal of Physical Oceanography*, 32(12), 3364–3375. [https://doi.org/10.1175/1520-0485\(2002\)032<3364:mmoowb>2.0.co;2](https://doi.org/10.1175/1520-0485(2002)032<3364:mmoowb>2.0.co;2)
- Banner, M. L., Babanin, A. V., & Young, I. (2000). Breaking probability for dominant waves on the sea surface. *Journal of Physical Oceanography*, 30(12), 3145–3160. [https://doi.org/10.1175/1520-0485\(2000\)030<3145:bpfdwo>2.0.co;2](https://doi.org/10.1175/1520-0485(2000)030<3145:bpfdwo>2.0.co;2)
- Barclay, D. R. (2022). 04). Oceanography by ear. *Journal of the Acoustical Society of America*, 151(4), R7–R9. <https://doi.org/10.1121/10.0009957>
- Belka, D., Schwendeman, M., Thomson, J., & Cronin, M. (2014). Historical wave and wind observations at ocean station p (Tech. Rep. No. 1407). *Applied Physics Laboratory*.
- Benetazzo, A., Halsne, T., Breivik, Ø., Strand, K. O., Callaghan, A. H., Barbariol, F., et al. (2024). On the short-term response of entrained air bubbles in the upper ocean: A case study in the North adriatic sea. *Ocean Science*, 20(3), 639–660. <https://doi.org/10.5194/os-20-639-2024>
- Brumer, S. E., Zappa, C. J., Brooks, I. M., Tamura, H., Brown, S. M., Blomquist, B. W., et al. (2017). Whitecap coverage dependence on wind and wave statistics as observed during so gasex and hiwings. *Journal of Physical Oceanography*, 47(9), 2211–2235. <https://doi.org/10.1175/JPO-D-17-0005.1>
- Callaghan, A. H., Deane, G. B., Stokes, M. D., & Ward, B. (2012). Observed variation in the decay time of oceanic whitecap foam. *Journal of Geophysical Research*, 117(C9), C09015. <https://doi.org/10.1029/2012JC008147>
- Callaghan, A. H., Stokes, M. D., & Deane, G. B. (2014). The effect of water temperature on air entrainment, bubble plumes, and surface foam in a laboratory breaking-wave analog. *Journal of Geophysical Research: Oceans*, 119(11), 7463–7482. <https://doi.org/10.1002/2014JC010351>
- CDIP. (2024). Data furnished by the coastal data information program (cdip), integrative oceanography division, operated by the scripps institution of oceanography, under the sponsorship of the u.s. army corps of engineers and the California department of parks and recreation. <https://doi.org/10.18437/C7WC72>
- Cifuentes-Lorenzen, A., Zappa, C. J., Randolph, K., & Edson, J. B. (2023). Scaling the bubble penetration depth in the ocean. *Journal of Geophysical Research: Oceans*, 128(9), e2022JC019582. <https://doi.org/10.1029/2022JC019582>
- Cronin, M. F., Anderson, N. D., Zhang, D., Berk, P., Wills, S. M., Serra, Y., et al. (2023). Pmel ocean climate stations as reference time series and research aggregate devices. *Oceanography*. <https://doi.org/10.5670/oceanog.2023.224>
- Cronin, M. F., Pelland, N. A., Emerson, S. R., & Crawford, W. R. (2015). Estimating diffusivity from the mixed layer heat and salt balances in the north pacific. *Journal of Geophysical Research: Oceans*, 120(11), 7346–7362. <https://doi.org/10.1002/2015JC011010>
- Czerski, H., Brooks, I. M., Gunn, S., Pascal, R., Matei, A., & Blomquist, B. (2022). Ocean bubbles under high wind conditions – Part 1: Bubble distribution and development. *Ocean Science*, 18(3), 565–586. <https://doi.org/10.5194/os-18-565-2022>
- D'Asaro, E. A., Thomson, J., Shcherbina, A. Y., Harcourt, R. R., Cronin, M. F., Hemer, M. A., & Fox-Kemper, B. (2014). Quantifying upper ocean turbulence driven by surface waves. *Geophysical Research Letters*, 41, 1–6. <https://doi.org/10.1002/2013GL058193>
- Davis, J., Thomson, J., Houghton, I. A., Doyle, J. D., Komaromi, W., Fairall, C. W., et al. (2023). Saturation of ocean surface wave slopes observed during hurricanes. *Geophysical Research Letters*, 50(16). <https://doi.org/10.1029/2023GL104139>
- Deane, G. B. (2000). Long time-base observations of surf noise. *Journal of the Acoustical Society of America*, 107(2), 758–770. <https://doi.org/10.1121/1.428259>
- Deane, G. B., & Stokes, M. D. (2002). Scale dependence of bubble creation mechanisms in breaking waves. *Nature*, 418(6900), 839–844. <https://doi.org/10.1038/nature00967>
- Derakhti, M., Thomson, J., Bassett, C., Malila, M., & Kirby, J. T. (2024). Statistics of bubble plumes generated by breaking surface waves. *Journal of Geophysical Research: Oceans*, 129(5), e2023JC019753. <https://doi.org/10.1029/2023JC019753>
- Dobson, F., Perrie, W., & Toulany, B. (1989). On the deep-water fetch laws for wind-generated surface gravity waves. *Atmosphere-Ocean*, 27(1), 210–236. <https://doi.org/10.1080/07055900.1989.9649334>
- Dragan-Górska, A., Górska, N., Markuszewski, P., & Klusek, Z. (2023). Influence of wind and waves on ambient noise and bubble entrainment depth in the semi-enclosed baltic sea. *Oceanologia*, 66(2), 299–318. <https://doi.org/10.1016/j.oceanog.2023.12.003>
- Farmer, D., & Vagle, S. (1988). On the determination of breaking surface wave distributions using ambient sound. *Journal of Geophysical Research*, 93(C4), 3591–3600. <https://doi.org/10.1029/JC093iC04p03591>
- Farmer, D. M., & Lemon, D. D. (1984). The influence of bubbles on ambient noise in the ocean at high wind speeds. *Journal of Physical Oceanography*, 14(11), 1762–1778. [https://doi.org/10.1175/1520-0485\(1984\)014<1762:TIOBOA>2.0.CO;2](https://doi.org/10.1175/1520-0485(1984)014<1762:TIOBOA>2.0.CO;2)
- Farmer, D. M., & Vagle, S. (1989). Waveguide propagation of ambient sound in the ocean-surface bubble layer. *Journal of the Acoustical Society of America*, 86(5), 1897–1908. <https://doi.org/10.1121/1.398568>
- Felizardo, F., & Melville, W. (1995). Correlation between ambient noise and the ocean surface wave field. *Journal of Physical Oceanography*, 25(4), 513–532. [https://doi.org/10.1175/1520-0485\(1995\)025<0513:cbanat>2.0.co;2](https://doi.org/10.1175/1520-0485(1995)025<0513:cbanat>2.0.co;2)
- Fontaine, E. (2012). A theoretical explanation of the fetch- and duration-limited laws. *Journal of Physical Oceanography*, 43(2), 233–247. <https://doi.org/10.1175/JPO-D-11-0190.1>
- Freeland, H. (2007). A short history of Ocean Station Papa and line P. *Progress in Oceanography*, 75(2), 120–125. <https://doi.org/10.1016/j.pocean.2007.08.005>
- Harrison, C. (1997). Canary: A simple model of ambient noise and coherence. *Applied Acoustics*, 51(3), 289–315. [https://doi.org/10.1016/s0003-682x\(97\)00004-2](https://doi.org/10.1016/s0003-682x(97)00004-2)
- Hasselmann, K., Barnett, T. P., Bouws, E., Carlson, H., Cartwright, D. E., Enke, K., et al. (1973). Measurements of wind-wave growth and swell decay during the joint north sea wave project (jonswap). *Ergänzungsheft zur Deutschen Hydrographischen Zeitschrift, Reihe A*.
- Hildebrand, J. A., Frasier, K. E., Baumann-Pickering, S., & Wiggins, S. M. (2021). 06). An empirical model for wind-generated ocean noise. *Journal of the Acoustical Society of America*, 149(6), 4516–4533. <https://doi.org/10.1121/10.0005430>
- Kleiss, J. M., & Melville, W. K. (2010). The analysis of sea surface imagery for whitecap kinematics. *Journal of Atmospheric and Oceanic Technology*, 28(2), 219–243. <https://doi.org/10.1175/2010JTECH0744.1>
- Kuperman, W. A., & Ingenito, F. (1980). Spatial correlation of surface generated noise in a stratified ocean. *Journal of the Acoustical Society of America*, 67(6), 1988–1996. <https://doi.org/10.1121/1.384439>
- Lemon, D. D., Farmer, D. M., & Watts, D. R. (1984). Acoustic measurements of wind speed and precipitation over a continental shelf. *Journal of Geophysical Research*, 89(C3), 3462–3472. <https://doi.org/10.1029/jc089ic03p03462>

- Malila, M. P., Thomson, J., Breivik, Ø., Benetazzo, A., Scanlon, B., & Ward, B. (2022). On the groupiness and intermittency of oceanic whitecaps. *Journal of Geophysical Research: Oceans*, 127(1), e2021JC017938. <https://doi.org/10.1029/2021JC017938>
- Manasseh, R., Babanin, A. V., Forbes, C., Rickards, K., Bobevski, I., & Ooi, A. (2006). Passive acoustic determination of wave-breaking events and their severity across the spectrum. *Journal of Atmospheric and Oceanic Technology*, 23(4), 599–618. <https://doi.org/10.1175/JTECH1853.1>
- Medwin, H., & Beaky, M. (1989). Bubble sources of the knudsen sea noise spectra. *Journal of the Acoustical Society of America*, 86(3), 1124–1130. <https://doi.org/10.1121/1.398104>
- Melville, W. K., & Matusov, P. (2002). Distribution of breaking waves at the ocean surface. *Nature*, 417(6884), 58–63. <https://doi.org/10.1038/417058a>
- Monahan, E. (1993). Occurrence and evolution of acoustically relevant sub-surface bubble plumes and their associated, remotely monitorable, surface whitecaps. In *Natural physical sources of underwater sound: Sea surface sound* (pp. 503–517). Springer Netherlands.
- Monahan, E., & Lu, M. (1990). Acoustically relevant bubble assemblages and their dependence on meteorological parameters. *IEEE Journal of Oceanic Engineering*, 15(4), 340–349. <https://doi.org/10.1109/48.103530>
- Na, B., Chang, K.-A., Huang, Z.-C., & Lim, H.-J. (2016). Turbulent flow field and air entrainment in laboratory plunging breaking waves. *Journal of Geophysical Research: Oceans*, 121(5), 2980–3009. <https://doi.org/10.1002/2015JC011377>
- Peláez-Zapata, D., Pakrashi, V., & Dias, F. (2024). Dynamics of bubble plumes produced by breaking waves. *Journal of Physical Oceanography*, 54(10), 2059–2071. <https://doi.org/10.1175/JPO-D-23-0261.1>
- Phillips, O. M. (1985). Spectral and statistical properties of the equilibrium range in wind-generated gravity waves. *Journal of Fluid Mechanics*, 156(-1), 495–531. <https://doi.org/10.1017/s0022112085002221>
- Pierson, W. J., & Moskowitz, L. (1964). A proposed spectral form for fully developed wind seas based on the similarity theory of A. A. Kitaigorodskii. *Journal of Geophysical Research*, 69(24), 5181–5190. <https://doi.org/10.1029/jz069i024p05181>
- Portilla-Yandún, J., Salazar, A., & Cavaleri, L. (2016). Climate patterns derived from ocean wave spectra. *Geophysical Research Letters*, n/a–n/a, 43(22). <https://doi.org/10.1002/2016GL071419>
- Schwendeman, M., & Thomson, J. (2015). Observations of whitecap coverage and the relation to wind stress, wave slope, and turbulent dissipation. *Journal of Geophysical Research: Oceans*, 120(12), 8346–8363. <https://doi.org/10.1002/2015JC011196>
- Schwendeman, M., Thomson, J., & Gemmrich, J. (2014). Wave breaking dissipation in a young wind sea. *Journal of Physical Oceanography*, 44(1), 104–127. <https://doi.org/10.1175/jpo-d-12-0237.1>
- Stiassnie, M. (2012). Fetch-limited growth of wind waves. *Journal of Geophysical Research*, 117(C11). <https://doi.org/10.1029/2011JC007579>
- Strand, K. O., Breivik, Ø., Pedersen, G., Vikebø, F. B., Sundby, S., & Christensen, K. H. (2020). Long-term statistics of observed bubble depth versus modeled wave dissipation. *Journal of Geophysical Research: Oceans*, 125(2), e2019JC015906. <https://doi.org/10.1029/2019JC015906>
- Sutherland, P., & Melville, W. K. (2013). Field measurements and scaling of ocean surface wave-breaking statistics. *Geophysical Research Letters*, n/a–n/a, 40(12), 3074–3079. <https://doi.org/10.1002/grl.50584>
- Thomson, J. (2012). Wave breaking dissipation observed with SWIFT drifters. *Journal of Atmospheric and Oceanic Technology*, 29(12), 1866–1882. <https://doi.org/10.1175/JTECH-D-12-00018.1>
- Thomson, J. (2024). Data related to “Surface wave development and ambient sound in the ocean.” Retrieved from <http://hdl.handle.net/1773/51039>
- Thomson, J., D’Asaro, E. A., Cronin, M., Rogers, E., Harcourt, R., & Scherbina, A. (2013). Waves and the equilibrium range at Ocean Weather station P. *Journal of Geophysical Research*, 118(11), 1–12. <https://doi.org/10.1002/2013JC008837>
- Thomson, J., & Jessup, A. (2009). A fourier-based method for the distribution of breaking crests from video observations. *Journal of Atmospheric and Oceanic Technology*, 26(8), 1663–1671. <https://doi.org/10.1175/2009JTECHO622.1>
- Thomson, J., Jessup, A., & Gemmrich, J. (2009). Energy dissipation and the spectral distribution of whitecaps. *Geophysical Research Letters*, 36(11). <https://doi.org/10.1029/2009gl038201>
- Thomson, J., Zeiden, K., James, M., LeClair, M., Moulton, M., Hosekova, L., et al. (2024). SASlabgroup/SWIFT-codes: V2024. *Zenodo*. <https://doi.org/10.5281/zenodo.13922183>
- Thomson, J., & Rogers, W. E. (2014). Swell and sea in the emerging Arctic ocean. *Geophysical Research Letters*, 41(9), 3136–3140. <https://doi.org/10.1002/2014GL059983>
- Thomson, J., Talbert, J., de Klerk, A., Brown, A., Schwendeman, M., Goldsmith, J., et al. (2015). Biofouling effects on the response of a wave measurement buoy in deep water. *Journal of Atmospheric and Oceanic Technology*, 32(6), 1281–1286. <https://doi.org/10.1175/JTECH-D-15-0029.1>
- Urick, R. J. (1975). *Principles of underwater sound*. McGraw-Hill.
- Vagle, S., Large, W., & Farmer, D. (1990). An evaluation of the WOTAN technique for inferring oceanic wind from underwater sound. *Journal of the Acoustical Society of America*, 7(4), 576–595. [https://doi.org/10.1175/1520-0426\(1990\)007<0576:aeotwt>2.0.co;2](https://doi.org/10.1175/1520-0426(1990)007<0576:aeotwt>2.0.co;2)
- Voermans, J. J., Babanin, A. V., Thomson, J., Smith, M. M., & Shen, H. H. (2019). Wave attenuation by sea ice turbulence. *Geophysical Research Letters*, 46(12), 6796–6803. <https://doi.org/10.1029/2019GL082945>
- Wenz, G. (1962). Acoustic ambient noise in the ocean: Spectra and sources. *Journal of the Acoustical Society of America*, 34(12), 1936–1956. <https://doi.org/10.1121/1.1909155>
- Wilson, J. (1983). Wind-generated noise modeling. *Journal of the Acoustical Society of America*, 73(1), 211–216. <https://doi.org/10.1121/1.388841>
- Yang, J., Nystuen, J. A., Riser, S. C., & Thorsos, E. I. (2023). Open ocean ambient noise data in the frequency band of 100 hz to 50 khz from the pacific ocean. *JASA Express Letters*, 3(3), 036001. <https://doi.org/10.1121/10.0017349>